

# Impact of weak localization on wave dynamics: Crossover from quasi-1D to slab geometry

Z.Q. Zhang,<sup>1</sup> S.K. Cheung,<sup>1</sup> X. Zhang,<sup>1</sup> A.A. Chabanov,<sup>2</sup> and A.Z. Genack<sup>2</sup>

<sup>1</sup>*Department of Physics, Hong Kong University of Science and Technology, Clear Water Bay, Kowloon, Hong Kong*

<sup>2</sup>*Department of Physics, Queens College of the City University of New York, Flushing, New York 11367, USA*

(Dated: November 19, 2018)

We study the dynamics of wave propagation in nominally diffusive samples by solving the Bethe-Salpeter equation with recurrent scattering included in a frequency-dependent vertex function, which renormalizes the mean free path of the system. We calculate the renormalized time-dependent diffusion coefficient,  $D(t)$ , following pulsed excitation of the system. For cylindrical samples with reflecting side walls and open ends, we observe a crossover in dynamics in the transformation from a quasi-1D to a slab geometry implemented by varying the ratio of the radius,  $R$ , to the length,  $L$ . Immediately after the peak of the transmitted pulse,  $D(t)$  falls linearly with a nonuniversal slope that approaches an asymptotic value for  $R/L \gg 1$ . The value of  $D(t)$  extrapolated to  $t = 0$ , depends only upon the dimensionless conductance  $g$  for  $R/L \ll 1$  and upon  $kl_0$  and  $L$  for  $R/L \gg 1$ , where  $k$  is the wave vector and  $l_0$  is the bare mean free path.

PACS numbers:

## I. INTRODUCTION

Weak localization (WL) of electronic and classical waves arises from the interference of counterpropagating partial waves in closed loops. Its impact upon electronic conductance [1] has been widely studied using steady-state methods such as magnetoresistance [2], and can be directly visualized as enhanced retroreflection of light from random samples [3]. Partial waves with trajectories over a wide range of lengths contribute to these phenomena. Most of the studies in the past were focused on the static transport properties. For instance, for a bulk system, WL makes all states localized in one and two dimensions. In three dimensions, it renormalizes the diffusion constant and can lead to the Anderson localization transition when the Ioffe-Regel criterion  $k\ell < 1$  is met, where  $k$  is the wave vector and  $\ell$  is the mean free path [4]. It is of great interest to investigate the variation of WL in the time domain [5, 6, 7, 8, 9]. Since the impact of WL increases with pathlength, which is proportional to time, it can dictate the dynamical behavior of wave propagation in a finite-sized sample. Though it has not been practical to isolate paths of specific lengths in studies of electronic conductance, this can be accomplished for classical waves in time-resolved measurements of pulsed transmission through random media [9, 10, 11, 12, 13, 14]. Time-resolved transmission measurements [10, 11] have generally been consistent with diffusion theory, which predicts a simple exponential decay of the average transmission. The asymptotic decay rate due to leakage from the sample is  $1/t_D = \pi^2 D_0 / (L + 2z_0)^2$ , where  $t_D$  is the diffusion time,  $D_0$  is the diffusion coefficient,  $L$  is the sample thickness, and  $z_0$  is the extrapolation length. Recently, however, Chabanov *et al.* [9] observed nonexponential decay of pulsed microwave transmission in a quasi-1D sample which was characterized via a “time-dependent diffusion coefficient,”  $D(t)$ . In fact, nonexponential behavior has been predicted for electronic systems. It was predicted that, when time is much greater than the Heisenberg time,  $t_H = \pi^2 g t_D$ , where  $g$  is the dimensionless conductance, the decay of the electron survival probability follows a log-normal behavior due to the presence of prelocalized states arising from some rare configurations of disorder in the medium [5, 15]. Recently, in a supermatrix model calculation by Mirlin [8], an analytic expression has been found for the tail of the electron survival probability when  $t \ll t_H$ . For the case of the orthogonal ensemble, it can be expressed in term of a “time-dependent diffusion coefficient,”  $D(t)/D_0 = 1 - 2t/t_H$ . Although such a linear decay of  $D(t)$  was found in microwave experiments [9]; nevertheless,  $D(t)$  did not extrapolate to the bare diffusion coefficient at  $t = 0$  and the scaling behavior of the slope of  $D(t)$  did not agree with the above expression. Nonexponential decay of pulsed transmission has also been reported recently in numerical simulations in 2D [16] and in a self-consistent diffusion theory, which includes recurrent scattering [17].

In this work, we solve the Bethe-Salpeter equation with recurrent scattering included in a manner that satisfies the Ward Identity [18, 19] to obtain the average time-dependent intensity transmitted through a random sample following pulsed excitation. Recurrent scattering is treated in the framework of self-consistent localization theory [18, 19] and is included in a frequency-dependent vertex function, which renormalizes the mean free path of the system. We calculate the renormalized time-dependent diffusion coefficient,  $D(t)$ , following pulsed excitation. The sample is cylindrical with reflecting side walls and open ends. By changing the ratio of the longitudinal dimension  $L$  and the radius  $R$ , a continuous transition can be made between two key experimental geometries: a quasi-1D geometry

with  $L \gg R$ , which is commonly employed in microwave experiments, and a slab with  $L \ll R$ , which is the typical optical geometry. For the quasi-1D geometry, we find  $D(t)/D_0 = A - (2B/\pi^2 g t_D)t$  for  $t \ll t_H$ . The constant part,  $A$ , is universal, depending only on  $g$ , while  $B$  is nonuniversal and depends upon  $L/\ell_0$ , where  $\ell_0$  is the bare mean free path, as well as upon  $g$ . In the limit  $g \gg 1$  and  $L/\ell_0 \gg 1$ , our results coincide with supersymmetry calculations in Ref. [7]. For moderate values of  $g$ ,  $g \geq 5$ , our results are in agreement with experiment [9]. For the slab geometry,  $D$  approaches a nearly constant renormalized value, being equal to  $D_0(1 - 1.03/(k\ell_0)^2)$  in the limit  $L/\ell_0 \gg 1$ . This is close to the result of WL theory for a bulk system.

## II. THEORY

We consider a plane wave pulse normally incident on the front surface of a random sample at  $z = 0$ . We assume that there is no gain or absorption in the medium and that scattering is isotropic. The ensemble-averaged intensity  $\langle I(t, \mathbf{r}) \rangle$  within the sample is obtained from the Fourier Transform of the frequency correlation function of the scalar field  $C_\Omega(\omega; \mathbf{r}) = \langle \phi_{\Omega^+}(\mathbf{r}) \phi_{\Omega^-}^*(\mathbf{r}) \rangle$ , i.e.,

$$\langle I(t, \mathbf{r}) \rangle = \frac{1}{2\pi} \int d\omega \exp(-i\omega t) C_\Omega(\omega; \mathbf{r}), \quad (1)$$

where  $\Omega^\pm = \Omega \pm \omega/2$ ,  $\Omega$  is the central frequency,  $\omega$  is the modulation frequency and  $\phi_\Omega(\mathbf{r})$  is the wave field at position  $\mathbf{r}$  inside the sample. In fact, it was Prof. George Papanicolaou who pointed out the importance of this frequency correlation function in the study of wave dynamics in randomly layered media [20, 21, 22].  $C_\Omega(\omega; \mathbf{r}) = \langle \phi_{\Omega^+}(\mathbf{r}) \phi_{\Omega^-}^*(\mathbf{r}) \rangle$ , is obtained from the space-frequency correlation function  $C_\Omega(\omega; \mathbf{r}, \mathbf{r}') = \langle \phi_{\Omega^+}(\mathbf{r}) \phi_{\Omega^-}^*(\mathbf{r}') \rangle$ , which satisfies the following Bethe-Salpeter equation,

$$\begin{aligned} C_\Omega(\omega; \mathbf{r}, \mathbf{r}') &= \langle \phi_{\Omega^+}(\mathbf{r}) \rangle \langle \phi_{\Omega^-}^*(\mathbf{r}') \rangle \\ &+ \int d\mathbf{r}_1 d\mathbf{r}_2 d\mathbf{r}_3 d\mathbf{r}_4 \langle G_{\Omega^+}(\mathbf{r}, \mathbf{r}_1) \rangle \langle G_{\Omega^-}(\mathbf{r}', \mathbf{r}_3) \rangle \\ &\times U_\Omega(\omega; \mathbf{r}_1, \mathbf{r}_2; \mathbf{r}_3, \mathbf{r}_4) C_\Omega(\omega; \mathbf{r}_2, \mathbf{r}_4), \end{aligned} \quad (2)$$

where  $\langle \phi_\Omega(\mathbf{r}) \rangle$  is the coherent source inside the sample, and  $\langle G_\Omega(\mathbf{r}, \mathbf{r}_1) \rangle = -\frac{\exp(i\kappa|\mathbf{r}-\mathbf{r}_1|)}{4\pi|\mathbf{r}-\mathbf{r}_1|}$  is the ensemble-averaged Green's function that represents the coherent part of wave propagation from  $\mathbf{r}_1$  to  $\mathbf{r}$ . The complex wavevector  $\kappa = k + \frac{i}{2\ell}$  describes the ballistic propagation inside the random media, where  $k = \frac{\Omega}{v}$  is the wavevector,  $v$  is the phase velocity, and  $\ell$  is the scattering mean free path, which is determined from the imaginary part of the self-energy of  $\langle G \rangle$ . In the absence of weak localization, the bare mean free path,  $\ell_0$ , is determined from the single-scattering diagram via  $\ell_0 = 1/n\sigma$ , where  $n$  is the density of scatterers and  $\sigma$  is the total scattering cross section. The vertex function  $U_\Omega$  represents the sum of all irreducible vertices. Here we approximate  $U_\Omega$  as

$$\begin{aligned} U_\Omega(\omega; \mathbf{r}_1, \mathbf{r}_2; \mathbf{r}_3, \mathbf{r}_4) &= \\ &\frac{4\pi}{\ell_0} [1 + \delta(\omega, k)] \delta(\mathbf{r}_1 - \mathbf{r}_2) \delta(\mathbf{r}_1 - \mathbf{r}_3) \delta(\mathbf{r}_1 - \mathbf{r}_4). \end{aligned} \quad (3)$$

The first term in the vertex function with a scattering strength  $4\pi/\ell_0$  represents self-avoiding paths and generates all the ladder diagrams that give rise to wave diffusion when  $L \gg \ell_0$  [23]. It is worth mentioning that in the absence of the second term Eq. (2) is equivalent to the radiative transport equation, which has been extensively used by Prof. George Papanicolaou in the study of multiple scattering in random media [24]. The second term with a vertex strength  $4\pi\delta(\omega, k)/\ell_0$  represents WL contribution to the vertex function. The presence of this term renormalizes the bare mean free path to a frequency-dependent mean free path, i.e.,  $\ell(\omega, k) = \ell_0/[1 + \delta(\omega, k)]$ . For flux conservation to hold, the Ward Identity [18, 19] requires that the mean free path  $\ell$  that appears in  $\langle G \rangle$  should also be replaced by the same  $\ell(\omega, k)$ . Since the second term represents recurrent scatterings, it is obtained by summing all maximally-crossed diagrams due to weak localization in the tube geometry. The assumption of point-like scattering for the WL contribution is justified as long as the system is far from the localization threshold, so that the renormalized mean free path is scale independent. In a bulk, the renormalization factor  $\delta(\omega, k)$  can be obtained from the renormalized diffusion coefficient [19], which can be written as

$$\frac{1}{D(\omega, k)} = \frac{1}{D_0} \left[ 1 + \frac{2\pi v}{k^2} \tilde{G}(\omega; \mathbf{r}, \mathbf{r}) \right], \quad (4)$$

where  $D(\omega, k) = v\ell(\omega, k)/3$ , and  $\tilde{G}$  is the Green's function that satisfies the diffusion equation in the frequency domain:

$$(D_0\nabla^2 + i\omega)\tilde{G}(\omega; \mathbf{r}, \mathbf{r}') = -\delta(\mathbf{r} - \mathbf{r}'), \quad (5)$$

The diagonal term of the Green's function,  $\tilde{G}(\omega; \mathbf{r}, \mathbf{r}')$ , represents the return probability of waves that travel diffusively inside the sample. For the geometry considered here, we solve for  $\tilde{G}$  by using the boundary conditions for a tube of radius  $R$  and length  $L$ , with perfectly reflecting cylindrical wall and open ends. The result can be written as

$$\tilde{G} = \tilde{G}_1 + \tilde{G}_2, \quad (6)$$

with

$$\tilde{G}_1(\omega; z = z') = \frac{2}{\pi R^2 \tilde{L}} \sum_{n=1}^{n_c} \frac{\sin^2[q_n(z + z_0)]}{-i\omega + D_0 q_n^2} \quad (7)$$

and

$$\begin{aligned} \tilde{G}_2(\omega; z = z') &= \frac{1}{2\pi D_0 \tilde{L}} \sum_{n=1}^{n_c} \sin^2[q_n(z + z_0)] \\ &\times \ln \left[ \frac{-i\omega + D_0(q_n^2 + \alpha^2/\ell_0^2)}{-i\omega + D_0(q_n^2 + 1/R^2)} \right], \end{aligned} \quad (8)$$

where  $q_n = n\pi/\tilde{L}$  is the transverse momentum,  $n_c = \alpha\tilde{L}/\pi\ell_0$  is the upper momentum cutoff in the z-direction,  $\tilde{L} = L + 2z_0$  is the effective length of the sample and  $z_0 = 0.7104\ell_0$  is the extrapolation length [4]. The factor  $\alpha/\ell_0$  in Eq. (8) denotes the upper momentum cutoff in the transverse direction.  $\alpha$  is chosen as 1 in our calculations unless otherwise specified. The  $\tilde{G}_1$  term arising from all the diffusive modes that are uniform in the transverse direction, i.e.,  $\tilde{q}_\perp = 0$ , is responsible for the continuous change of decay rate in the ensemble-averaged transmitted intensity  $\langle I(t) \rangle$ . The existence of this term is due to the reflecting boundary conditions at the cylindrical wall at which  $\nabla\tilde{G} = 0$  normal to the surface. The  $\tilde{G}_2$  term represents the contributions of the transverse modes other than  $\tilde{q}_\perp = 0$ . Here we have assumed that  $\tilde{G}_2$  is independent of the transverse position, which is valid when  $R \gg \ell_0$ . This term becomes important when  $2R/L$  is not small. In the limit of slab geometry, i.e.,  $2R/L \gg 1$ ,  $\tilde{G}_1$  is insignificant and  $\tilde{G}_2$  becomes the main contribution. Eqs. (7) and (8) indicate that the renormalized mean free path is z-dependent. In order to simplify our calculations, we take the spatial average along the z-axis and replace the factor of  $\sin^2[q_n(z + z_0)]$  by  $1/2$ . This simplification is valid as long as  $L \gg \ell_0$ . The self-consistent theory of WL requires us to replace  $D_0$  in Eq. (7) and (8) by  $D(\omega, k)$  [18, 19]. Using Eqs. (3,4,6-8), we finally obtain

$$\delta(\omega, k) = \delta_1(\omega, k) + \delta_2(\omega, k), \quad (9)$$

with

$$\delta_1(\omega, k) = \frac{v}{2N\tilde{L}} \sum_{n=1}^{n_c} \frac{1}{-i\omega + D(\omega, k)q_n^2} \quad (10)$$

and

$$\delta_2(\omega, k) = \frac{3}{2k^2\ell_0\tilde{L}} \sum_{n=1}^{n_c} \ln \left( \frac{-i\omega + D(\omega, k)(q_n^2 + \alpha^2/\ell_0^2)}{-i\omega + D(\omega, k)(q_n^2 + 1/R^2)} \right), \quad (11)$$

where  $N = (kR)^2/4$  is the number of transverse modes in the tube. Eq. (11) requires  $R > \ell_0/\alpha$ , otherwise,  $\delta_2(\omega = 0) < 0$ . In our calculations, we solve Eqs. (10) and (11) for  $\delta(\omega, k)$  self-consistently with  $D(\omega, k) = v\ell(\omega, k)/3 = v\ell_0/[3(1 + \delta(\omega, k))]$ . Physically, the self-consistency of  $\ell(\omega, k)$  or  $D(\omega, k)$  assures the continuous renormalization due to recurrent scattering paths. In the static limit and when  $L/\ell_0$  is large, it can be shown that  $\delta_1(\omega = 0) = 1/(3g - 1)$ , where  $g = 4N\ell_0/3\tilde{L}$  is the dimensionless conductance. This result implies that localization transition occurs at  $g = 1/3$  or  $N = \tilde{L}/4\ell_0$  in quasi-1D geometry.

In our calculation, we assume both the excitation intensity and the scattered intensity are uniform over the transverse cross-section of the tube. Eq. (1) can now be written as [14]

$$C_{\Omega}(\omega, z) = \exp\left(\frac{i\omega z}{v} - \frac{z}{\ell_0}\right) + \frac{1}{4\pi\ell(k, \omega)} \int_0^L dz' H(\omega, z - z') C_{\Omega}(\omega, z'), \quad (12)$$

where

$$H(\omega, z - z') = \pi \int d\rho^2 \times \frac{\exp\left[\left(\frac{i\omega}{v} - \frac{1}{\ell(\omega, k)}\right) \sqrt{\rho^2 + (z - z')^2}\right]}{\rho^2 + (z - z')^2}. \quad (13)$$

Eq. (12) is numerically solved for  $C_{\Omega}(\omega, z)$ . The transmitted intensity  $\langle I(t, L) \rangle$  is then calculated from the Fourier transform of  $C_{\Omega}(\omega, L)$ , from which we obtain the renormalized time-dependent diffusion coefficient by using the relation  $D(t)/D_0 = -\tau_D d \ln \langle I(t) \rangle / dt$ , for  $t > \tau_D$ , where  $\tau_D = \tilde{L}^2 / \pi^2 D_0$  is the diffusion time [9].

### III. RESULTS AND DISCUSSIONS

The time evolution of wave propagation is described by the renormalized diffusion coefficient  $D(t)/D_0$ , which, in turns, depends on the behavior of  $\delta(\omega)$ . Thus it is important to understand the general behaviors of  $\delta_1(\omega)$  and  $\delta_2(\omega)$ . In Fig. 1, we show the functions  $\delta_1(\omega)$  and  $\delta_2(\omega)$  for a typical case of  $k\ell_0 = 4$  and  $L = 20\ell_0$ . For  $\delta_1(\omega)$  we choose  $R = 3.5\ell_0$  ( $2R/L = 0.35$ ), which corresponds to  $N = 50$ . For  $\delta_2(\omega)$  we choose  $R$  as infinity, which corresponds to a slab geometry. The diffusion time in this case is  $\tau_D \cong 139\ell_0/v$ , which implies that the width of the frequency correlation function is,  $\delta\omega \cong 2\pi/\tau_D = 0.045$ . From Fig. 1, a shape rise in the real part of  $\delta_1(\omega)$  (curve a) is found when  $\omega < \delta\omega$ . This behavior suggests that significant renormalization of  $D(t)$  will occur when  $t > \tau_D$ . In fact, it is this sharp rise of  $\delta_1$  at small  $\omega$  that leads to the linear decay of  $D(t)$  found previously [8, 9]. However, the behavior of  $\delta_2(\omega)$  is very different from that of  $\delta_1(\omega)$ . The real part of  $\delta_2(\omega)$  (curve c) increases slowly with decreasing  $\omega$ . This suggests a gradual renormalization of  $D(t)$  and will lead to a nearly constant  $D(t)$  in the slab geometry. This is also consistent with the exponential decay of the transmitted intensity found previously in the optical measurements [12, 13].

In the inset of Fig. 1, we plot  $\delta_1(0)$ ,  $\delta_2(0)$  and  $\delta(0)$  as functions of  $2R/L$ . It is clear that  $\delta_1$  dominates when  $2R/L \ll 1$ . As  $2R/L$  is increased to 1,  $\delta_2$  becomes the dominant term. The saturation of  $\delta_2$  when  $2R/L > 2$  implies that the behavior of  $D(t)$  will not change much when  $2R/L > 2$ .

#### (a) quasi-1D system

For quasi-1D systems, we first compare our theory with the microwave experiments reported in Ref. [9]. The results are shown in Fig. 2 for  $N = 68$  and  $L/\ell_0 = 6.4$  (sample A), 9.5 (sample B), and 19.2 (sample C), corresponding to  $\ell_0 = 9.5$  cm. The best fit is found at  $\alpha = 0.5$ , and good agreement is found for Samples A and B. For Sample C, for which  $g = 3$ , however, our theory predicts a smaller decay rate, reflecting the important role of localization effects, which are not included here.

The linear region of the diffusion coefficient immediately after the peak can be fitted with  $D(t)/D_0 = A - Bt''$ , where  $t'' = 2t/\pi^2 g \tau_D$ . Mirlin's analytical result of Ref. [8] predicts  $A = B = 1$ . Nevertheless, our calculations [25] show that  $A$  is a universal function of  $g$  and can be fitted by a single curve  $A = 1.00 - 0.27/g - 0.17/g^2$ . In the limit of large  $g$ ,  $A$  approaches 1. However, the slope  $B$  depends on both  $g$  and  $L/\ell_0$ . For each value of  $L/\ell_0$ ,  $B$  can be fitted with  $B = B_0(L) + B_1(L)/g + B_2(L)/g^2$  with  $B_0(L)$  being a linear function of  $(\tilde{L}/\ell_0)^{-1}$ . In the limit of large  $L/\ell_0$ ,  $B_0$  approaches 0.96. Thus, our results indicates that the analytical expression of [8] is valid only when both  $g$  and  $L/\ell_0$  are sufficiently large.

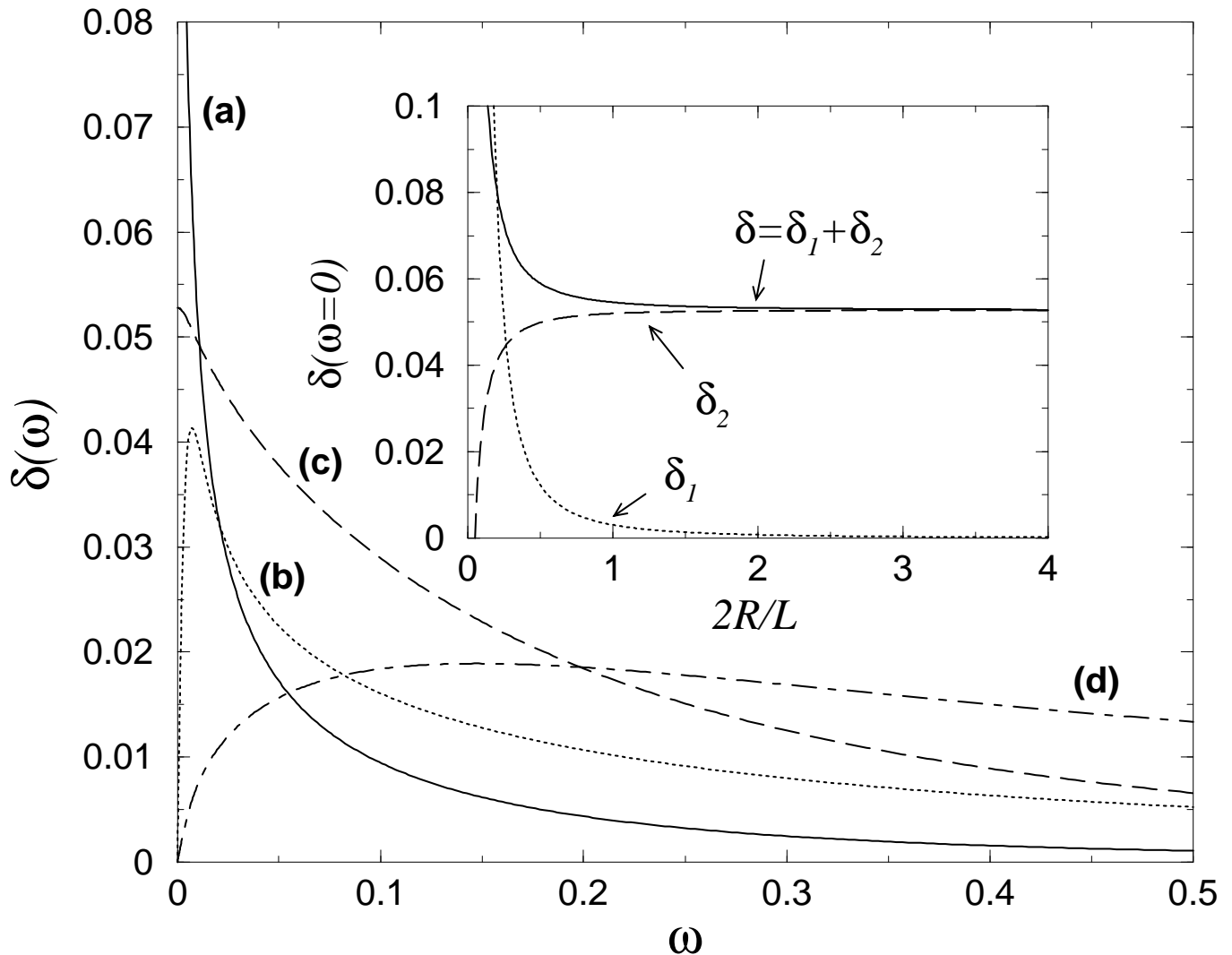


FIG. 1:  $\delta(\omega)$  with  $L = 20\ell_0$  and  $k\ell_0 = 4$  are plotted as functions of  $\omega$ . Here (a) is the real part and (b) is the imaginary part of  $\delta_1(\omega)$  when  $R = 3.5\ell_0$  ( $N = 50$ ), while (c) is the real part and (d) is the imaginary part of  $\delta_2(\omega)$  in the limit of  $R \rightarrow \infty$  (slab geometry). In the inset:  $\delta(\omega = 0)$ ,  $\delta_1(\omega = 0)$  and  $\delta_2(\omega = 0)$  for  $L = 20\ell_0$  and  $k\ell_0 = 4$  are plotted as a function of  $2R/L$ .

### (b) crossover from quasi-1D to slab geometry

It is interesting to see how the behavior of  $D(t)$  crosses over from a quasi-1D to a slab geometry as  $2R/L$  increases. A plot of  $D(t)/D_0$  as a function of dimensionless time  $t' = t/\tau_D$  at  $2R/L = 0.35, 0.5, 1, 2, 4$  and  $\infty$  (slab) is shown in Fig. 3 for the case  $L = 20\ell_0$  and  $k\ell_0 = 4$ . When  $2R/L = 0.35$ , the  $\delta_1$  term dominates and  $D(t)/D_0$  decreases rapidly between  $t \simeq 2t_D$  and  $15t_D$  and gradually saturates to a constant value at later times. As  $2R/L$  increases, the peak of  $D(t)/D_0$  near  $t \simeq 2 - 3t_D$  also increases. In the meantime, the decay of  $D(t)/D_0$  at later times is reduced. This indicates a smaller WL effect when  $2R/L$  is increased. This is consistent with the decrease of  $\delta(0)$  with  $2R/L$  shown in the inset of Fig. 1. When  $2R/L > 2$ ,  $D(t)/D_0$  approaches a constant value. This again is consistent with the saturation of  $\delta(0)$  when  $2R/L > 2$  shown in the inset of Fig. 1.

In order to give a systematic description of the crossover behavior, we present the crossover behavior of the intercept  $A$  obtained from the linear fit of  $D(t)/D_0$  immediately after the peak. In Fig. 4, we plot  $A$  as a function of  $g$  for different values of  $2R/L$  and for  $L/\ell_0 = 20$ . The data are well fit by  $A = A_0 + A_1/g + A_2/g^2$ . Thus, at large  $g$ , we have  $A = 1 - C_0(2R/L)/g$ , where  $C_0$  is an increasing function of  $2R/L$ . From the fit of the data (dashed lines), we find that  $C_0(2R/L)$  is proportional to  $R^2$  when  $2R/L > 1$ . This  $R^2$  dependence cancels the  $R^2$  factor in  $g$  in

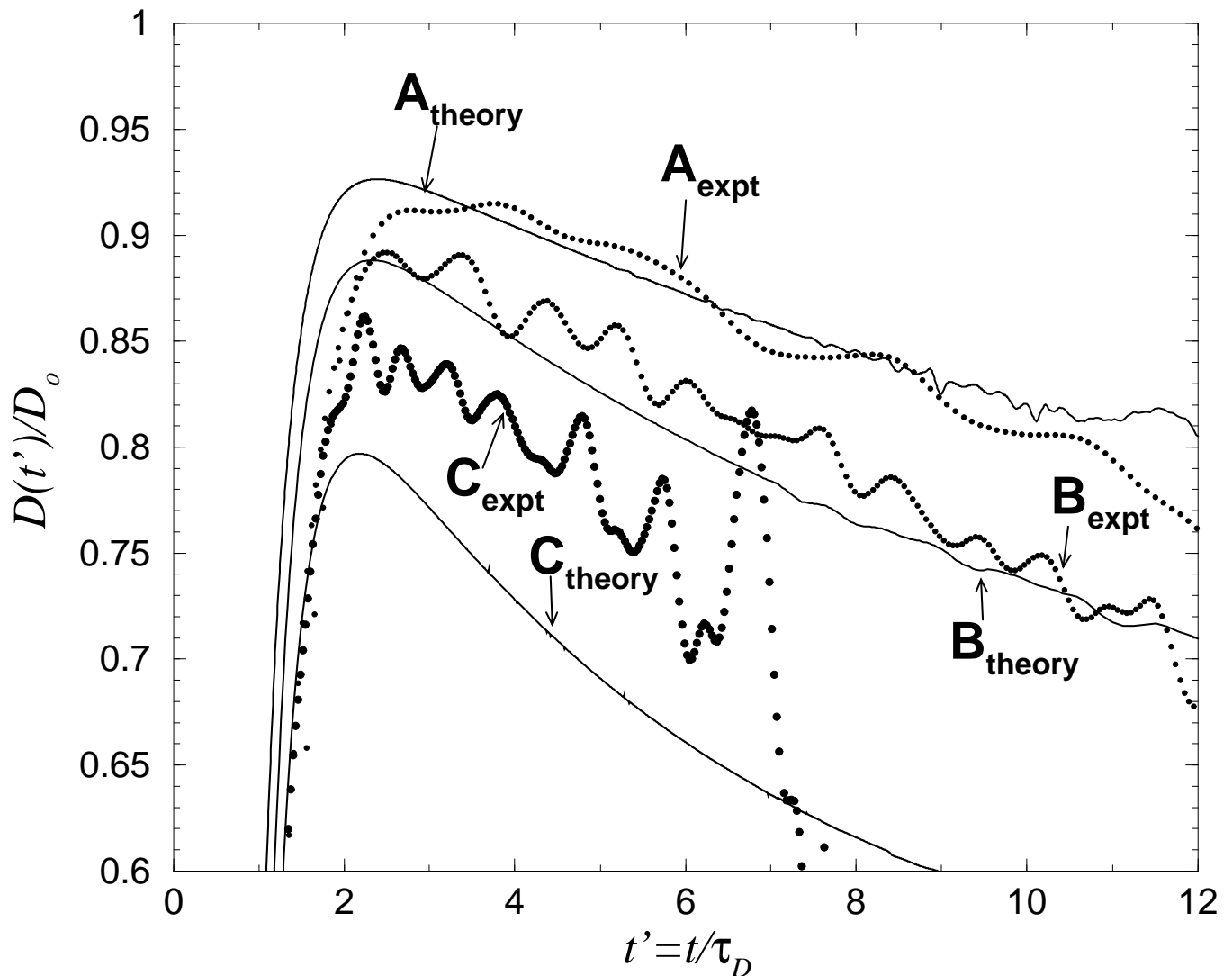


FIG. 2:  $D(t)/D_0$  is plotted as a function of  $t' = t/\tau_D$  for three samples studied in Ref. [9], with  $N = 68$ ,  $L/\ell_0 = 6.4$  (sample A), 9.5 (sample B) and 19.2 (sample C), where  $D_0 = 42.5\text{cm}^2/\text{ns}$ . The theoretical results for the corresponding samples are shown in solid lines.

the denominator. Thus, in the slab limit, we can write  $A = 1 - c(L)/(k\ell_0)^2$ . This behavior can also be seen from the inset of Fig. 4, where  $A$  is plotted as a function of  $2R/L$  for different values of  $k\ell_0$  for the case of  $L = 20\ell_0$ .  $A$  approaches a constant value when  $2R > L$  for each value of  $k\ell_0$ .

### (c) slab geometry

In order to find the function  $c(L)$  in  $A(k, L) = 1 - c(L)/(k\ell_0)^2$  for the slab, we plot  $A(k, L)$  as functions  $1/(k\ell_0)^2$  in Fig. 5 for different values of  $L/\ell_0$ . The slopes of these curves give  $c(L)$  and is shown in the inset of Fig. 5. Since  $c(L)$  is an increasing of  $L$ ,  $D(t)/D_0 \cong A$  decreases with  $L$ . This reflects continuous renormalization of the diffusion coefficient with increasing  $L$  due to the presence of longer recurrent scattering path lengths in a thicker sample. The fitting of the data of  $c(L)$  in the inset of Fig. 4 gives  $c(L) = 1.02 - 3.72\ell_0/\tilde{L}$ . Thus, we find  $D(t)/D_0 \cong 1 - 1.02/(k\ell_0)^2 + 3.72\ell_0/\tilde{L}(k\ell_0)^2$ . In the limit of large  $L$ , we recover the result of weak localization theory for the bulk, i.e.,  $D/D_0 = 1 - 3\alpha/\pi(k\ell_0)^2$  with  $\alpha = 1$  [19].

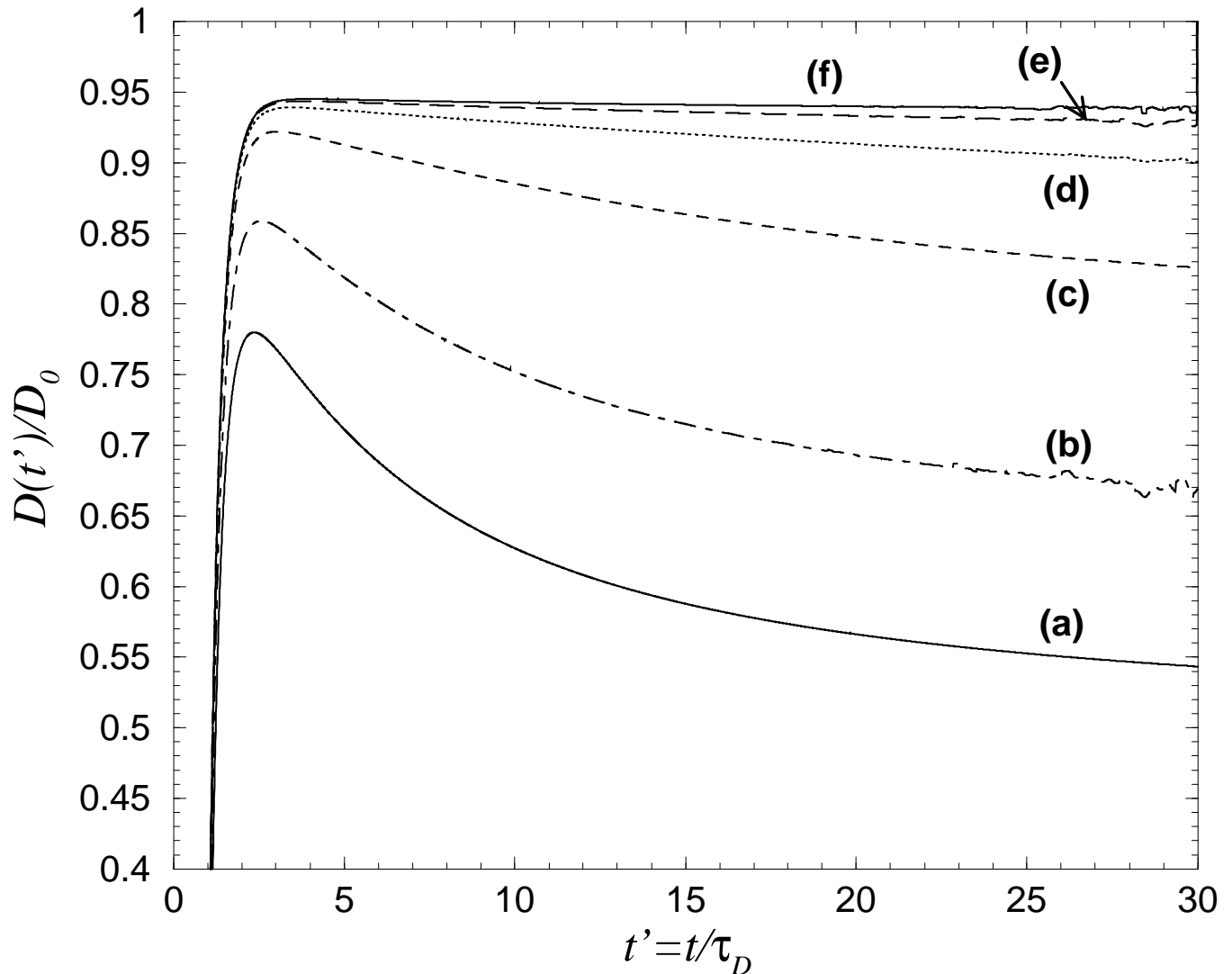


FIG. 3:  $D(t)/D_0$  is plotted as a function of  $t' = t/\tau_D$  for the case of  $L = 20\ell_0$  and  $k\ell_0 = 4$ , with (a)  $2R/L = 0.35$ , (b)  $2R/L = 0.5$ , (c)  $2R/L = 1$ , (d)  $2R/L = 2$ , (e)  $2R/L = 4$  and (f)  $2R/L \rightarrow \infty$  (slab).

#### IV. CONCLUSION

In conclusion, we have solved the Bethe-Salpeter equation with recurrent scattering to find the impact of WL on the dynamics of wave propagation through a finite-sized mesoscopic sample. The crossover from quasi-1D to slab geometry is studied through the change in the behavior of the time-dependent diffusion coefficient  $D(t)$  for different aspect ratio  $2R/L$ . In quasi-1D systems,  $D(t)$  decays rapidly immediately after the peak of the pulse is transmitted. In contrast,  $D(t)$  is nearly constant for a slab. These different behaviors are attributed to two different kinds of WL factors which appear in each case. These results are consistent with microwave [9] and optical [12, 13] measurements.

Discussions with P. Sheng are gratefully acknowledged. This research is supported by Hong Kong RGC Grant No. HKUST 6163/01P and NSF Grant No. DMR0205186.

---

[1] *Mesoscopic Phenomena in Solids*, edited by B.L. Altshuler, P.A. Lee, and R.A. Webb (North Holland, Amsterdam, 1991).

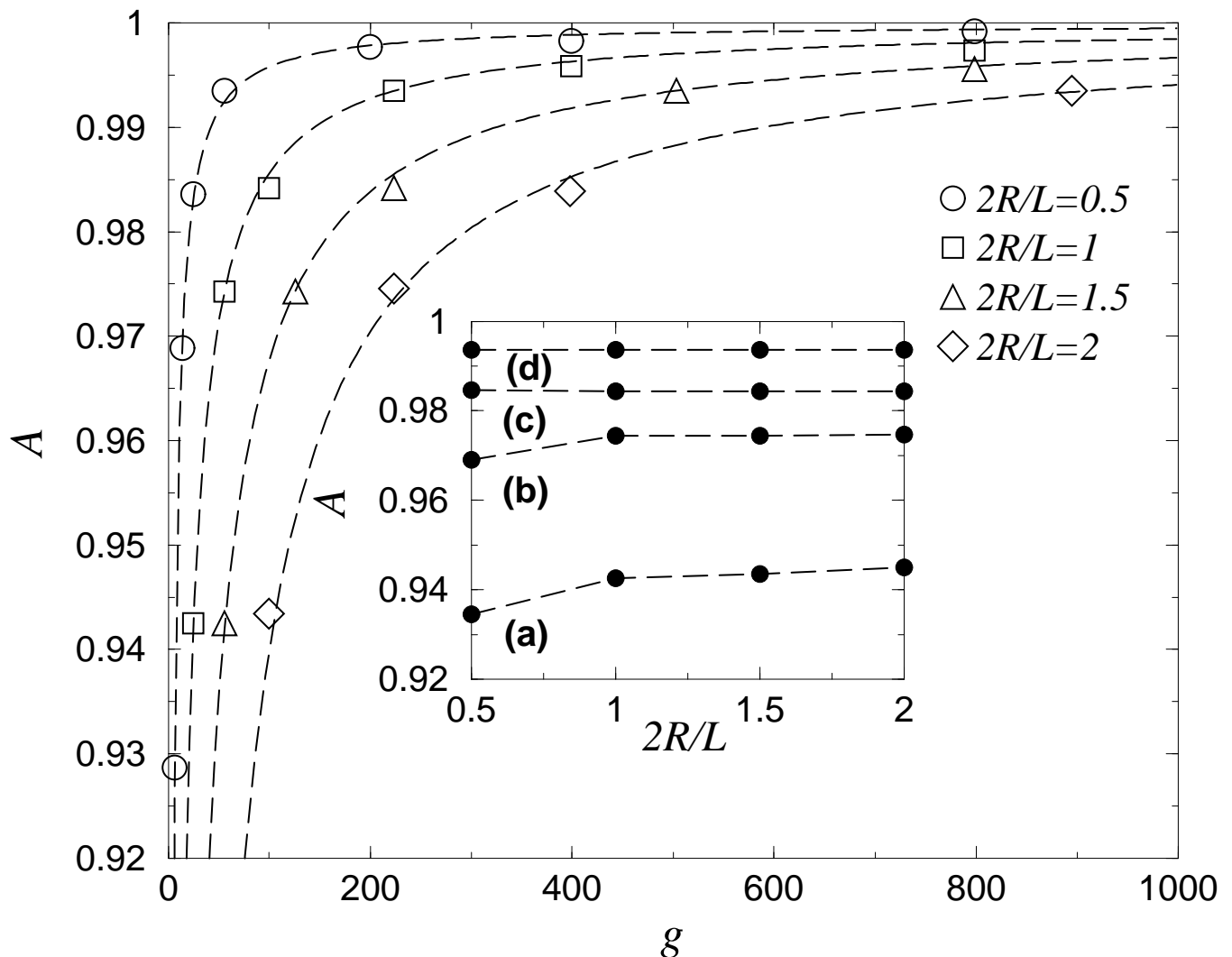


FIG. 4: The parameter  $A$  obtained from the fit of  $D(t'')/D_0$  with  $A - Bt''$  is plotted as a function of  $g$  for  $L/\ell_0 = 20$  and different aspect ratio  $2R/L$ . The dashed curves are the fit of  $A$  with  $A = A_0 + A_1/g + A_2/g^2$ , where  $A_i$  are constant. In the inset:  $A$  versus  $2R/L$  for  $k\ell_0 =$  (a) 4, (b) 6, (c) 8 and (d) 12.

- [2] G. Bergmann, Phys. Rep. **107**, 1 (1984).
- [3] M.P. van Albada and A. Lagendijk, Phys. Rev. Lett. **55**, 2692 (1985); P.E. Wolf and G. Maret, Phys. Rev. Lett. **55**, 2696 (1985); E. Akkermans, P.E. Wolf, and R. Maynard, Phys. Rev. Lett. **56**, 1471 (1986).
- [4] P. Sheng *Introduction to Wave Scattering, Localization and Mesoscopic Phenomena* (Academic, San Diego, 1995).
- [5] B.L. Altshuler, V.E. Kravtsov, and I.V. Lerner, in [1], and in Zh. Exp. Teor. Fiz. **45**, 160 (1987) ;**94**, 258 (1988); B.A. Muzykantskii and D.E. Khmelnitskii, Phys. Rev. B **51**, 5480 (1995).
- [6] R. Berkovits and M. Kaveh, J. Phys. Condens. Matter **2**, 307 (1990).
- [7] R.L. Weaver, Phys. Rev. B **49**, 5881 (1994).
- [8] A.D. Mirlin, Phys. Rep. **326**, 259 (2000).
- [9] A.A. Chabanov, Z.Q. Zhang, and A.Z. Genack, Phys. Rev. Lett. **90**, 203903 (2003).
- [10] G.H. Watson, Jr., P.A. Fleury, and S.L. McCall, Phys. Rev. Lett. **58**, 945 (1987).
- [11] J.M. Drake and A.Z. Genack, Phys. Rev. Lett. **63**, 259 (1989); A.Z. Genack and J.M. Drake, Europhys. Lett. **11**, 331 (1990).
- [12] K.M. Yoo, F. Liu, and R.R. Alfano, Phys. Rev. Lett. **64**, 2647 (1990).
- [13] R.H.J. Kop, P. deVries, R. Sprik, and A. Lagendijk, Phys. Rev. Lett. **79**, 4369 (1997).
- [14] Z.Q. Zhang, I.P. Jones, H.P. Schriemer, J.H. Page, D.A. Weitz, and P. Sheng, Phys. Rev. E **60**, 4843 (1999).
- [15] V.M. Apalkov, M.E. Raikh, and B. Shapiro, Phys. Rev. Lett. **89**, 016802 (2002).
- [16] M. Haney and R. Snieder, Phys. Rev. Lett. **91**, 093902 (2003).

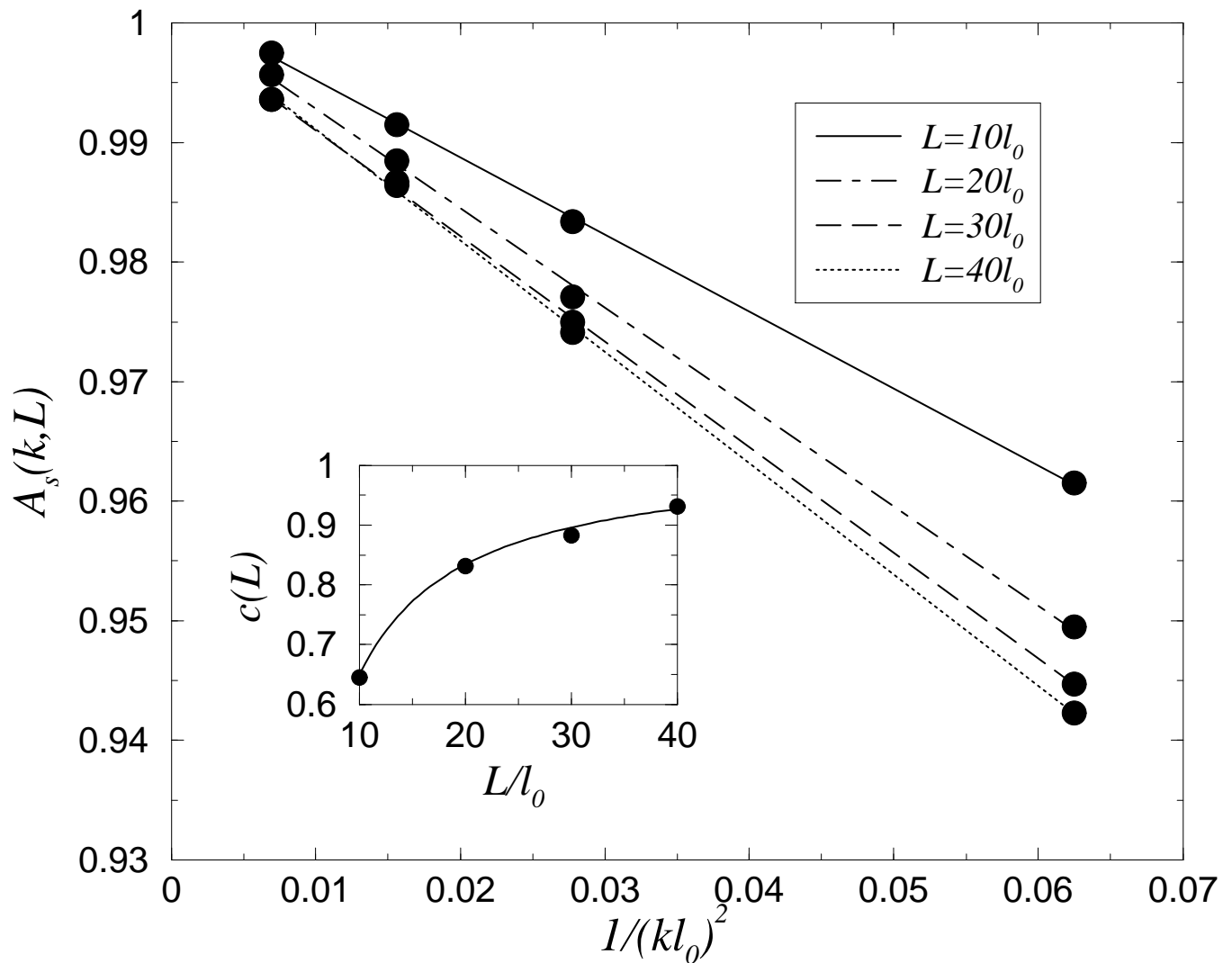


FIG. 5: The saturation values  $A_s(k, L)$  in large  $R$  obtained from the inset of Fig. 4 are plotted versus  $1/(kl_0)^2$  for the cases of  $L = 10l_0, 20l_0, 30l_0$  and  $40l_0$ . In the inset:  $c(L)$  is plotted as a function of  $L/l_0$ , which is obtained from the fit of the formula  $A_s(k, L) = 1 - c(L)/(kl_0)^2$ . The solid curve is the fit of the data points with the formula  $c(L) = 1.02 - 3.72l_0/\tilde{L}$ .

- [17] S.E. Skipetrov and B.A. van Tiggelen, *phys. Rev. Lett.* **92**, 113901 (2004).
- [18] D. Vollhardt and P. Wolfle, *Phys. Rev. B* **22**, 4666 (1980); *Phys. Rev. Lett.* **42**, 673 (1979).
- [19] T.R. Kirkpatrick, *Phys. Rev. B* **31**, 5746 (1985).
- [20] P. Sheng, Z.Q. Zhang, B. White, and G. Papanicolaou, *Phys. Rev. Lett.* **57**, 1000 (1986).
- [21] B. White, P. Sheng, Z.Q. Zhang, and G. Papanicolaou, *Phys. Rev. Lett.* **59**, 1918 (1987).
- [22] B. White, P. Sheng, Z.Q. Zhang, and G. Papanicolaou; *Scattering and Localization of Classical Waves in Random Media* (World Scientific Publishing 1990) P.563, Ed. P. Sheng.
- [23] M.B. van der Mark, M.P. van Albada and A. Lagendijk, *Phys. Rev. B* **37**, 3575 (1988).
- [24] For examples, W. Kohler and G. Papanicolaou, *J. Math. Phys.* **14**, 1733 (1973); *ibid* **15**, 2186 (1974); and L. Ryzhik, G. Papanicolaou, and J.B. Keller, *Wave Motion* **24**, 327 (1996).
- [25] S.K. Cheung, X.D. Zhang, Z.Q. Zhang, A.A. Chabanov and A.Z. Genack, *Phys. Rev. Lett.* **92**, 173902 (2004).